JOURNAL OF SOLID STATE CHEMISTRY 68, 320–329 (1987)

Electron Diffraction Evidence for Domain Structures in the Low-Temperature Incommensurate Phase in CuV_2S_4

J. MAHY

University of Antwerp, RUCA, Groenenborgerlaan 171, B-2020 Antwerp, Belgium

D. COLAITIS

ER 210, CNRS, 92190 Bellevue Meudon, France

D. VAN DYCK

University of Antwerp, RUCA, Groenenborgerlaan 171, B-2020 Antwerp, Belgium

AND S. AMELINCKX

University of Antwerp, RUCA, Groenenborgerlaan 171, B-2020 Antwerp, and CEN-SCK, 2400 Mol, Belgium

Received June 30, 1986; in revised form September 29, 1986

A low-temperature electron diffraction study of the sulfo spinel CuV_2S_4 is presented. From the diffraction geometry analysis a deformation modulated structure of the room temperature spinel phase below 90 K is proposed. Taking the low-temperature reflection intensities into account qualitatively, evidence is presented for a domain structure consisting of six orientation variants, corresponding with a symmetry lowering from cubic (order 48) to orthorhombic (order 8). The observation of pairs of low-temperature reflections located at incommensurate positions leads to a structure model consisting of quasi-periodically stacked antiphase boundaries characterized by a displacement vector $\mathbf{R} = \frac{1}{2}[101]$. The deformation modulation is interpreted in terms of dimerized $\langle 110 \rangle$ types of copper-atom zig-zag chains, possibly associated with a charge density wave-type distortion.

1. Introduction

The ternary sulfo spinel CuV_2S_4 was reported to exhibit an incommensurate superlattice associated with charge density wave (CDW) formation (*1*). Hitherto the presence of a CDW state, which was observed in several pseudo one- and two-dimensional compounds, could be established in a very limited number of "three-dimensional" cubic structures only.

The observed magnetic susceptibility and electronic resistivity revealed anomalous behavior associated with second-order displacive structural phase transitions, characteristic of a CDW state. These transitions at 90 and 75 K, respectively, were studied by means of X-ray diffraction techniques (*1*,

0022-4596/87 $3.00

2). The experiments showed the presence of an incommensurate superlattice at 90 K, which gradually locks-in into a commensurate one at 75 K. A first-order transition was also observed at around 50 K.

Further physical (thermopower and Hall effect) and spectroscopic (XPS) measurements confirmed these results (*2, 3*). They were interpreted in terms of a collective Jahn–Teller distortion mechanism acting on the vanadium and sulfur sublattices. Moreover a tetragonal lowering of the spinel symmetry was reported by X-ray powder diffractometry (*2, 3*), in apparent contradiction to the conservation of the cubic symmetry proposed by Fleming *et al.* (*1*).

In this work a low-temperature *in situ* electron microscopy study of the diffraction effects associated with the structural phase transitions in CuV_2S_4 are presented.

It is shown that the analysis of the geometry of diffraction patterns revealing incommensurate reflections could be carried out straightforwardly by the introduction of periodic arrays of interfaces in a deformation modulated structure. This method has been successfully applied in several structures ranging from composition modulated ordering systems (*4, 5*) to deformation modulated displacive systems (*6, 7*).

2. Crystal Structure

2.1. Room Temperature Structure

The symmetry of CuV_2S_4 (Fig. 1a) is described by the space group $Fd3m$ at room temperature (*8*). The cubic unit cell with $a = 9.8$ Å contains 32 S atoms in (*e*) positions; 16 V atoms in (*d*) positions, and 8 Cu atoms in (*a*) positions (*8*). Figure 1b shows a projection of the cubic unit cell along [001]. The Cu atoms are located in the centers of perfect S atom tetrahedra between layers consisting of edge-sharing S atom octahedra with the V atoms located in the centers of slightly distorted edge-sharing S atom octahedra. The structure can be considered as consisting of two interpenetrating sublattices: a diamond-type Cu sublattice (Fig. 1c) and a partly filled NaCl type V_2S_4 lattice. It is interesting to notice that the Cu sublattice can formally be regarded as consisting of zig-zag chains of Cu atoms along six ⟨110⟩ type directions. The vectors connecting adjacent Cu atoms along one chain are of the type $\frac{1}{4}\langle 111\rangle$. This can be seen clearly in the [1$\bar{1}$0] projection shown in Fig. 2.

2.2. Low-Temperature Modulation

Fleming *et al.* (*1*) reported the formation at 90 K of an incommensurate modulation wave with wave vector $\mathbf{q} = (\frac{1}{4} - \delta)[110]$, with the incommensurability δ gradually decreasing to 0 at 75 K. Strong second-order scattering $2\mathbf{q}$ was observed. At 50 K, the wave vector abruptly changes from $\frac{1}{4}[110]$ to $(\frac{1}{3} - \delta)[110]$. Moreover, Fleming *et al.* observed weak reflections at the (200), (600), and (420) Bragg positions below 50 K, which are forbidden in the spinel space group. Van Bruggen on the other hand (*2*) observed the splitting at 83 K of high-angle Bragg reflections (880) and (484).

3. Electron Diffraction Results

The low-temperature electron diffraction experiments were performed with the DEEKO 250 electron microscope at the Fritz Haber Institute in Berlin. This instrument combines both accurate temperature control and high thermal and high mechanical stability (low specimen drift) which is essential for observations of the same crystal area during temperature recycling (*9*). Moreover, a low-intensity beam was used to minimize irradiation damage by the 250-kV electrons required for the penetration of the samples.

The results are shown in Figs. 3 and 4. An accurately oriented [001] type zone was

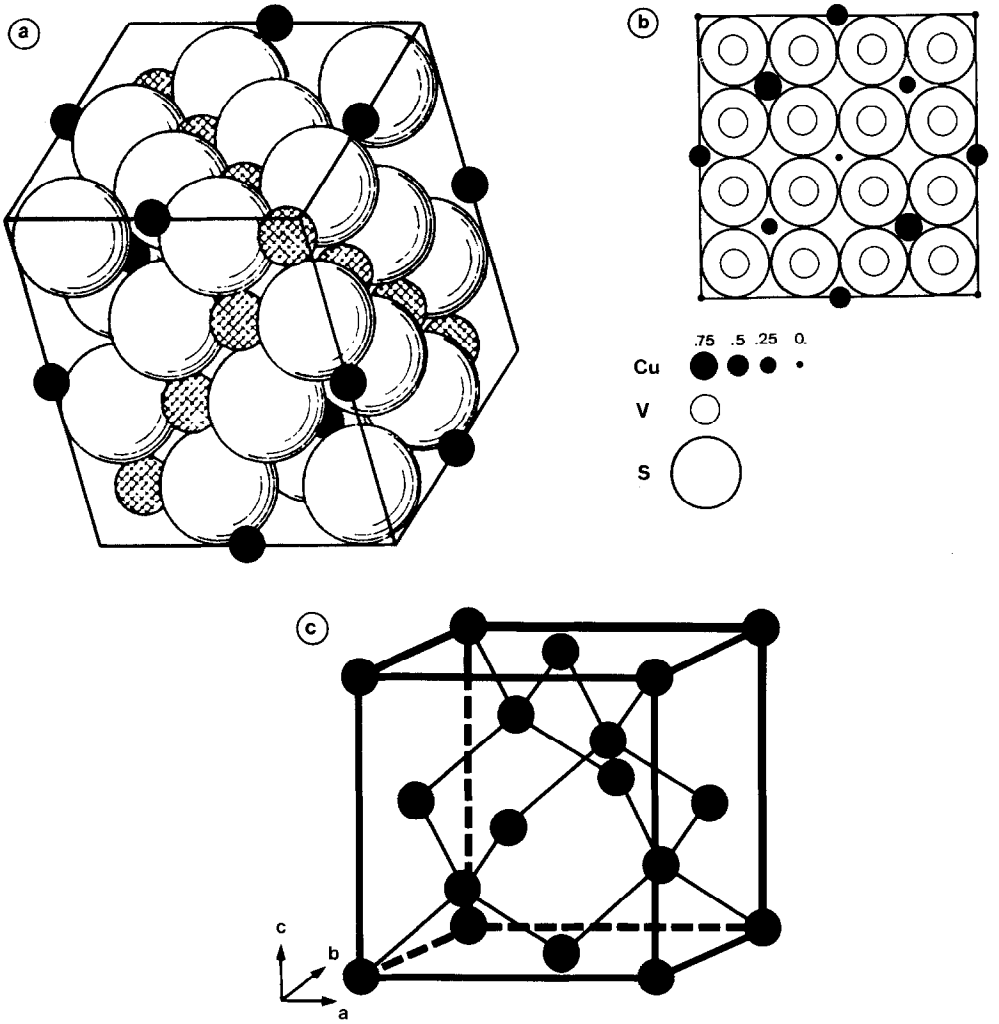

FIG. 1. Spinel structure. (a) CuV_2S_4 structure model; (b) [001] projection, showing the projected $a\sqrt{2}/4 \times a\sqrt{2}/4$ Cu sublattice unit cell; (c) Diamond type Cu sublattice. Large circles denote S, smaller ones V, and small solid ones Cu.

selected, showing the first-order Laue zones (FOLZ) apart from the zeroth order or basal [001] Laue zone (ZOLZ).

At room temperature (RT) all the observed reflections are those allowed by the symmetry of the $Fd3m$ space group. The reflections present in the [001] ZOLZ are of the type ($hk0$) with h and k even and $h + k = 4n$; i.e., their positions correspond with the reciprocal nodes of the Cu sublattice projected along the z axis, with an effective projected unit cell of a $\sqrt{2}/4 \times a\sqrt{2}/4$ as indicated in Fig. 1b.

On cooling the specimen, several phenomena are observed in the diffraction pattern. At about 150 K weak but sharp reflections appear at the kinematically forbidden positions ($hk0$) with h and k even and $h + k = 4n + 2$ of the ZOLZ (Fig. 3a). Upon cooling, their intensity increases, which may be an indication that they are not entirely due to multiple diffraction effects.

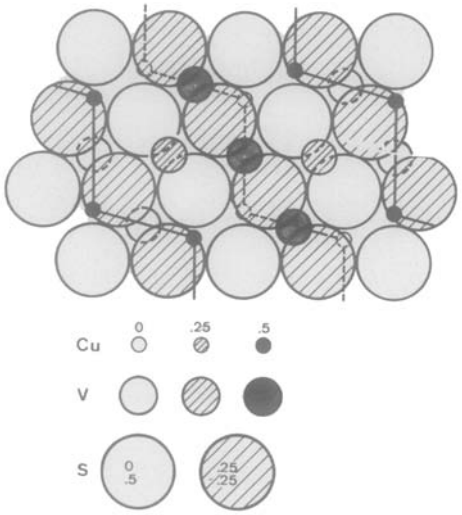

FIG. 2. A [110] projection of the CuV_2S_4 structure, showing zig-zag chains of Cu atoms along ⟨110⟩ directions.

At about 90 K diffuse intensity appears in the diffraction pattern (Fig. 3b) which on further cooling concentrates in sharp reflections visible in additional Laue zones, hereafter called the Laue subzones. At 70 K, sharp incommensurate reflections also appear in the ZOLZ (Fig. 3c) and below 50 K (Fig. 4) also in the FOLZ. Apart from the low-temperature (LT) spot intensities which increase relative to those of the RT reflections upon cooling (Fig. 3d), their (incommensurate) positions change as a function of temperature, as derived further on. However, even at the lowest temperature obtained (20 K), diffuse intensity remains between the Laue subzones. These phenomena were found to be reversible with temperature, although irradiation damage was observed after repeated temperature cycling.

Although the low-temperature diffraction patterns seem very complex, careful analysis shows that, apart from the forbidden reflections appearing at 150 K, all the LT reflections are apparently symmetry related as shown in Fig. 5. The reflections are located at positions incommensurate with the RT spinel phase at the corners of squares. These squares are explicitly drawn in Fig. 5 and serve as a visual guide without actually implying a relationship between spots belonging to the same square. The centers of the squares are located midway along the edges and at the face centers of the $2a^* \times 2a^* \times 2a^*$ reciprocal cell. The incommensurability, i.e., the ratio of the edge of the squares to the edge of the $2a^*$ cube, is not constant but changes from $\frac{1}{4} - \delta$ to $\frac{1}{3} - \delta$ upon cooling from approximately 90 to 20 K.

Apart from the diffraction geometry analysis, leading to the reconstruction of reciprocal space as represented in Fig. 5, the diffracted intensities were considered also, although on a more qualitative level. In the [001] zone diffraction pattern several types of rows of closely spaced pairs of LT reflections can be distinguished. For instance, the Laue subzones around $c^*/3$ and $2c^*/3$ consist of ⟨100⟩* types of rows, whereas in the zero level layer Laue zone that LT reflections are arranged on ⟨110⟩* types of rows. For both types two perpendicular directions are present within the [001] zone.

Upon cooling at around 90 K systematic differences in intensity between the ⟨100⟩* type rows are observed as shown in Figs. 3b and 3c. These differences become more pronounced around 70 K, where the ⟨110⟩* type rows also appear. The latter reveal similar intensity differences for both perpendicular directions. At around 20 K the ⟨100⟩* as well as the ⟨110⟩* type rows have become equally intense (Fig. 3d). However, the observation of ⟨100⟩* type rows located in the Laue subzone around $2c^*/3$ shows a more subtle phenomenon. Adjacent reflections along one such row show alternating intensities (Fig. 4). Furthermore, neighboring ⟨100⟩* rows are in antiphase with respect to the spot intensity alternation. A schematic representation in which Ewald's sphere effects have been omitted (which are important for the large-

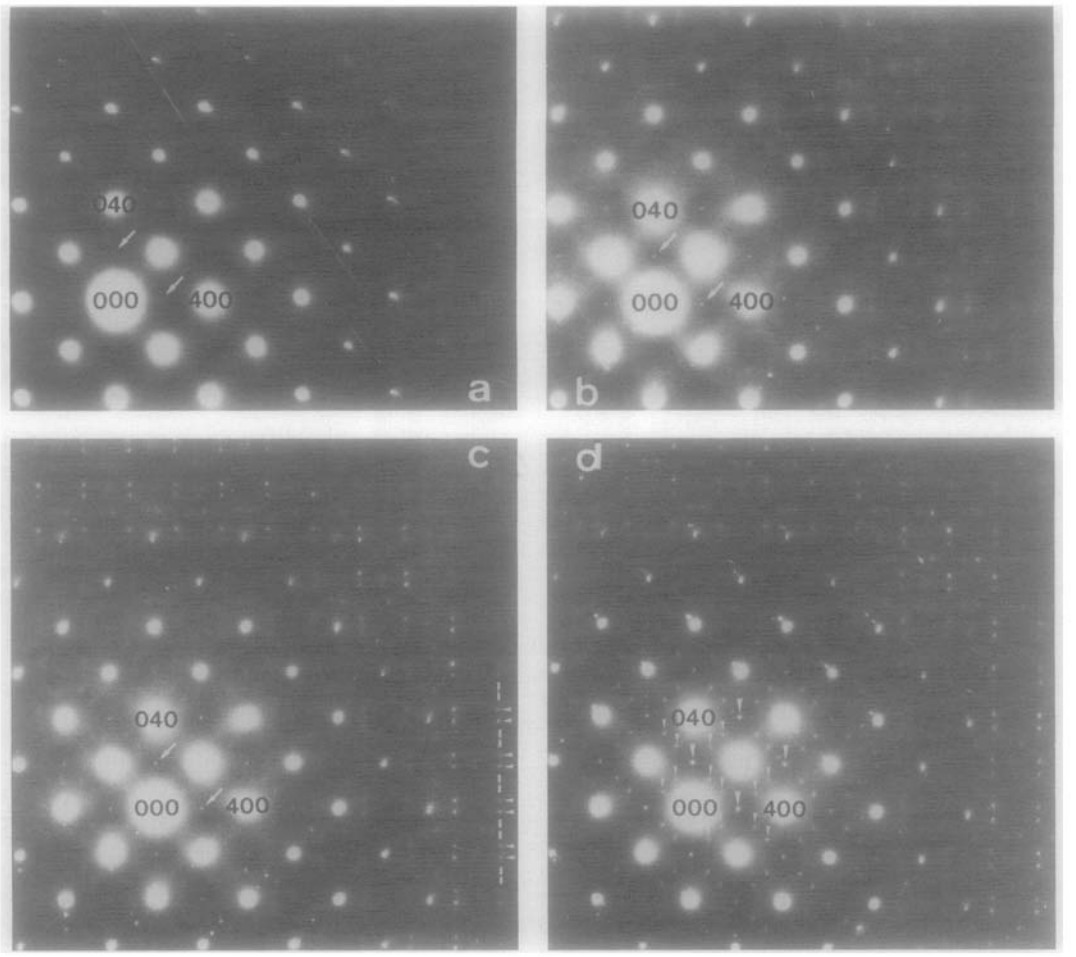

FIG. 3. Electron diffraction patterns along the [001]* zone. (a) At 150 K the spinel forbidden ($hk0$) reflections with h, k even and $h + k = 4n + 2$ appear in the zero level Laue zone (arrows). (b) At 90 K the diffuse intensity is piling up in spots along the ⟨100⟩* directions in Laue subzones. (c) At 70 K the perpendicular ⟨100⟩* rows show systematic intensity differences. (d) At 20 K the ⟨110⟩* rows of LT reflections in zero level Laue zone, as well as the ⟨100⟩* rows in Laue subzones, are equally intense. Forbidden reflections are sharp and intense.

angle reflections under consideration) is shown in Fig. 6. It is assumed generally that all subzones of the type $2nc^*/3$ exhibit these alternating intensities, whereas $(2n + 1)c^*/3$ subzones do not. From Fig. 5 it then follows that systematic intensity differences only occur for LT reflections located on the "squares" centering the $2a^*$ cube faces and not for those centering the $2a^*$ cube edges.

The ZOLZ also contains LT reflections located on face-centered "squares" as diagonally opposed spots. Moreover only two out of four possible LT reflections on a square are present in the ZOLZ, showing no markedly differing intensities. Therefore spots located at $2a^*$ cube face centering squares are proposed to be generated in diagonally opposed pairs. Each intense spot in the $2c^*/3$ subzone thus belongs to a pair,

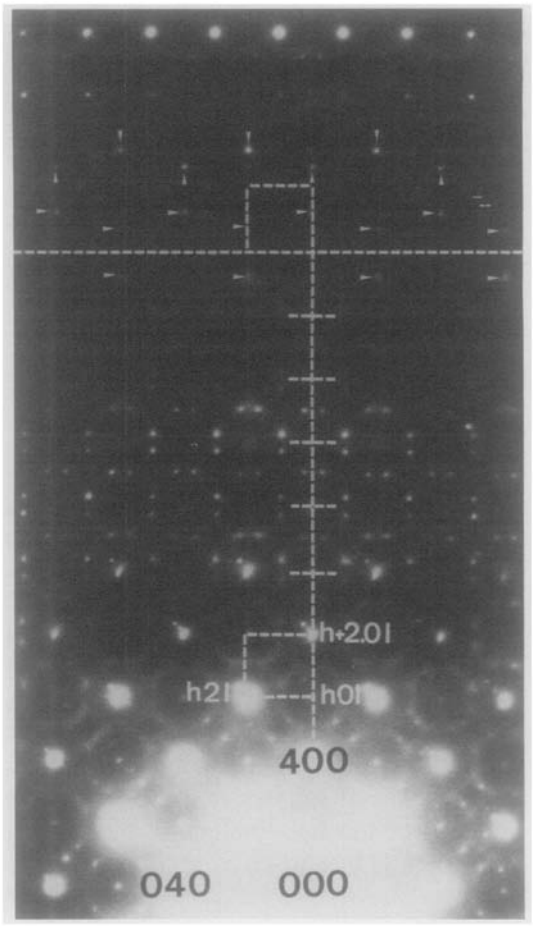

FIG. 4. An electron diffraction pattern along the [001]* zone showing zero and first level Laue zones as well as subzones around $c^*/3$ and $2c^*/3$. The latter reveals systematically alternating reflection intensities along the $\langle 100\rangle^*$ directions (arrows indicate intense reflection in a pair) associated with orientation variants. The dashed lines show "mapping" of reciprocal $2a^*$ cube reciprocal lattice.

the other member of which is located in the $4c^*/3$ subzone (which is not visible, however).

4. Interpretation

From the qualitative considerations presented above, the reciprocal space model of Fig. 5 can be regarded as a superposition of

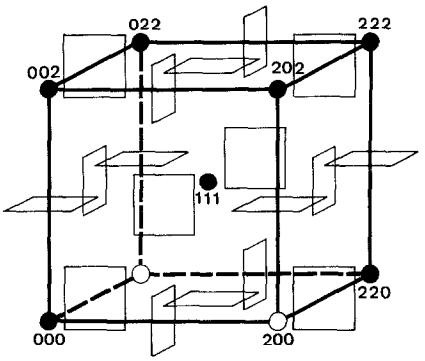

FIG. 5. Model for the reciprocal space. Squares indicate positions where LT reflections are located at their corners. Open circles indicate ZOLZ extinctions.

symmetry related diffraction patterns. Since there are three possible mutually perpendicular orientations of the LT spot squares centering a $2a^*$ cube face, and since each such square consists of two pairs of spots, six pair orientations are possible. From the foregoing considerations it follows that each such pair is independent from the others from intensity arguments, and belongs to separate reciprocal spaces. This leads us naturally to postulate the occurrence of six possible orientation variants. The reciprocal space model derived for one of these variants is represented in Fig. 7 (only the pairs oriented along $[\bar{1}10]^*$ are considered).

A structure model for this variant will be

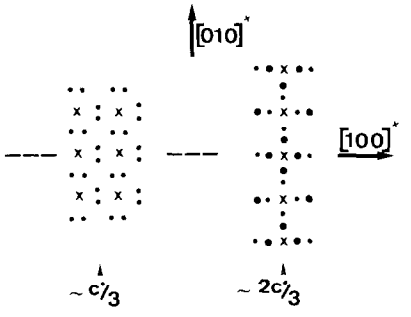

FIG. 6. A schematic representation of the $2c^*/3$ subzone systematic intensity differences along $\langle 100\rangle^*$ rows of LT spot pairs. Crosses indicate $2a^*$ cube projection.

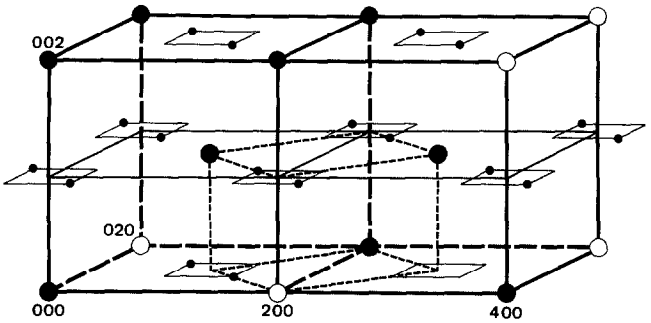

FIG. 7. Model for the reciprocal space associated with a single orientation variant showing pairs of LT spots diagonally opposed on square corners. Reciprocal lattice associated with hypothetical "basic" structure shown in dashed lines.

constructed using the "interface modulated structure" approach originally developed for shear structures and periodic defect structures in ordering systems (*11, 10, 4*). In this approach, the "superlattice" reflections are considered as originating from basic reflections by the introduction of periodic arrays of planar interfaces or antiphase boundaries (APB). Denoting **R** the displacement vector of the APB and d their separation, the superlattice reflection array {**h**} associated with the positions {**H**} of the reflections of the "basic", i.e., an unfaulted structure, is given by

$$\mathbf{h} = \mathbf{H} + 1/d(m - \mathbf{H} \cdot \mathbf{R})\mathbf{e} \quad m = \text{integer},$$

where **e** is the unit vector normal to the APB. The interspot spacing therefore equals $1/d$ and the array of superlattice reflections is shifted with respect to **H** over $\mathbf{H} \cdot \mathbf{R}/d$. If the periodicity is not perfect, d represents the average separation of the APB so that the superlattice reflection positions can be (pseudo-) incommensurate with the reciprocal lattice of the unfaulted structure. With increasing disorder the width of the reflection intensity profiles increases whereas the intensities of possible higher order reflections decreases (*11*). This unfaulted structure can be hypothetical, however; that is, it might never be observed without APBs being present.

As a consequence of the theory outlined in the previous paragraph the LT spots associated with one variant can be regarded as being caused by the introduction of a quasi-periodic array of APB in the hypothetical structure. Conversely, the reciprocal lattice associated with this hypothetical structure will thus consist of nodes located midway between the LT spot pairs, i.e., in the centers of the $2a^*$ cube faces perpendicular to [001]*, and the $2a^*$ cube edges parallel to [001]*. It follows that the reciprocal unit cell of the hypothetical structure can conveniently be chosen as $\sqrt{2}a^* \times \sqrt{2}a^* \times a^*$.

Since from the analysis of the diffraction geometry no information on the actual atomic arrangements can be obtained, it will be assumed that the distortion mainly affects the Cu sublattice. This assumption is justified by the observation that the symmetry of the LT spot configuration is the same as for the diamond type copper sublattice.

The volume of the $\sqrt{2}a^* \times \sqrt{2}a^* \times a^*$ reciprocal unit cell is twice that of the $a^* \times a^* \times a^*$ spinel reciprocal unit cell which contains eight Cu atoms in its associated real space cell. The real space unit cell is then tetragonal with lattice parameters $(\sqrt{2}/2)a \times (\sqrt{2}/2)a \times a$ and contains four Cu atoms. This cell is shown in Fig. 9.

Some symmetry restrictions for the displacements of the four independent copper

atoms within this tetragonal cell follow from the observation of the extinction conditions in the reciprocal space associated with one variant, and taking into account that if a LT spot pair is extinct the corresponding spot of the hypothetical structure is extinct also. From Fig. 7 it then follows that the displacements projected along [001] of the copper atoms labeled 1 and 2 as well as for 3 and 4 in Fig. 9 are the same.

Considering successive Cu atoms along, e.g., $[\bar{1}10]$ zig-zag chains, the atoms are allowed to be grouped pairwise along these chains, the projection of the pair (1,3) being identical to that of (2,4) along [001] (Fig. 9). Taking into account further that the zig-zag chains are symmetry related, it can be concluded that both (1,3) and (2,4) pairs are physically identical and mirror related with respect to the (100) plane.

Preliminary kinematical structure factor calculations for typical atom displacements of the order of 0.01 nm along the ⟨111⟩ type symmetry axis of the copper "dimer" yield good qualitative agreement with the intensities of the observed pairs of LT spots. Such ⟨111⟩ direction displacements moreover lead to nonextinct (hkl) reflections with h and k even and $h + k = 4n + 2$ in the $l = 2$ zone, as observed.

The LT spot pairs are generated by introducing {110} type APBs in the hypothetical (unfaulted) structure. Obviously one set of parallel {110} planes is parallel with only one set of ⟨110⟩ zig-zag chains. The displacement vector **R** interconnecting distorted regions across the APB can be derived from the fractional shift **H** · **R** (mod. 1) of the LT spot pairs with respect to the nodes {**H**} of the hypothetical reciprocal lattice. It is seen to be either zero or $\frac{1}{2}$. The vector $\mathbf{R} = \frac{1}{2}[111]_b$ can easily be derived from Table I. It is indexed with respect to the basic structure and becomes $\mathbf{R} = \frac{1}{2}[011]$ in the spinel structure. This vector is indeed a vector of the projected diamond lattice and not of the basic hypothetical lattice, as expected.

TABLE I

H	**H** · **R** (mod. 1) observed	**R** = $[uvw]$
(100)	$\frac{1}{2}$	$u = \frac{1}{2}$(mod. 1)
(001)	$\frac{1}{2}$	$w = \frac{1}{2}$(mod. 1)
(101)	0	$u + w = 0$(mod. 1)
(111)	$\frac{1}{2}$	$u + v + w = \frac{1}{2}$(mod. 1) $v = \frac{1}{2}$(mod. 1)

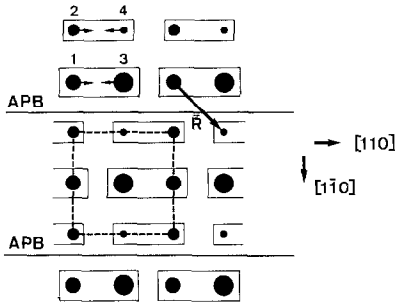

FIG. 8. Model for the APB modulated "basic" (hypothetical) structure projected along [001] showing Cu dimers (in rectangles) with possible displacement indicated by arrows. APB introduces shift over $\mathbf{R} = \frac{1}{2}[101]$. Projection of dimers (1,3) and (2,4) are identical. Basic structure projection shown in dashed lines.

The separation of the APB is necessarily an integral number of times the projected interchain spacing $(\sqrt{2}/4)a$. It is seen from the interspot distance to be about $0.27(2a^*\sqrt{2}) = 1/d$ which gives $d \simeq 1.3a \simeq 3.7$ $((\sqrt{2}/4)a)$. Consequently this spacing can be regarded as an average APB separation, which is a mixing of $3((\sqrt{2}/4)a)$ and $4((\sqrt{2}/4)a)$ separations (Fig. 8).

5. Discussion

The six orientation variants are related by the same symmetry relation as the ⟨110⟩ zig-zag chains, i.e., a $\bar{3}$ axis. The variants can all be described by three tetragonal unit cells, their unique axes along ⟨100⟩ directions. Each tetragonal unit cell contains four Cu atoms which can be displaced so as to form two possible sets of dimers, for in-

stance, the sets (1,2) and (3,4) rather than (1,3) and (2,4) in Fig. 9.

The hypothetical distorted but unfaulted structure has a point group symmetry $2/m$ $2/m$ $2/m$ of order 8, as compared to the spinel symmetry $4/m\ \bar{3}\ 2/m$ of order 48. The real quasi-periodic APB modulated structure is described by an effective unit cell of three or four hypothetical ones arranged along ⟨110⟩ (Fig. 8). The question whether or not the APB can be considered as abrupt two-dimensional interfaces, or rather as an extended region, cannot be answered, however, since the diffraction geometry remains unaffected by the detailed shape of the APB. In this way their description in terms of "discommensurations" (*12*) could be favorable, although no conclusive evidence for phase soliton behavior of the distortion is yet available.

Moreover, although the LT spot positions were observed to shift as a function of temperature, indicating a redistribution of the APB separations, no actual lock-in transformation typical for a CDW state was noted down to 20 K. Possibly the electron beam irradiation prevents the nucleation of the lock-in phase. Irradiation damage was indeed observed to destroy the LT spot configuration after a few (reversible) cooling/heating cycles, or after intense electron beam focusing.

The fact that the ZOLZ spots occur at slightly lower temperatures than the LT subzone reflections might be related to thin foil effects, which would cause a preferential nucleation of one variant above others (*13*). This in turn could be associated with the tetragonal symmetry lowering reported by Refs. (*2, 3*) which is not in contradiction with the present work.

Finally it is pointed out that the spinel-forbidden reflections ($hk0$) with h and k even and $h + k = 4n + 2$, which were also observed by Fleming *et al.* (*1*), are generally found to be heavily affected by multiple diffraction effects (*14*). Although such effects are important in electron diffraction, it is pointed out that their intensity increased dramatically upon cooling, indicating a genuine symmetry lowering of the spinel phase. The existence of a domain structure of orientation variants could in principle be established directly by means of dark field electron microscopy. However, preliminary experiments in which only LT spots were selected for image formation were unsuccessful in revealing a domain structure, probably due to the very low beam intensities used, as required to avoid irradiation damage. Additional dark field imaging and low-temperature X-ray structure refinement experiments are planned.

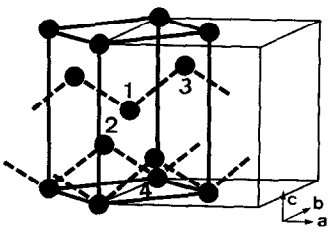

FIG. 9. Model for the hypothetical distorted Cu sublattice (bold lines) showing Cu zig-zag chains (dashed lines) and spinel unit cell (thin lines).

Acknowledgments

The authors thank Dr. C. F. Van Bruggen for stimulating discussions. To Professor E. Zeitler and Dr. Y. Uchida of the Fritz Haber Institute in Berlin they express their gratitude for the availability of and assistance with the DEEKO 250 microscope.

References

1. R. M. FLEMING, F. J. J. DISALVO, R. J. CAVA, AND J. V. WASZCZAK, *Phys. Rev. B* **24**, 2850 (1981).
2. C. F. VAN BRUGGEN, *Ann Chim. Fr.* **7**, 171 (1982).
3. R. A. BERGER AND C. F. VAN BRUGGEN, *Stud. Inorg. Chem.* **3**, 663 (1983).
4. D. COLAÏTIS, P. DELAVIGNETTE, D. VAN DYCK, AND S. AMELINCKX, *Phys. Status Solidi A* **51**, 657 (1979).

5. D. COLAÏTIS, D. VAN DYCK, AND S. AMELINCKX, *Phys. Status Solidi A* **68,** 419 (1981).
6. J. MAHY, J. VAN LANDUYT, S. AMELINCKX, Y. UCHIDA, K. D. BRONSEMA, AND S. VAN SMAALEN, *Phys. Rev. Lett.* **55,** 11, 1188 (1985).
7. J. MAHY, J. VAN LANDUYT, S. AMELINCKX, K. D. BRONSEMA, AND S. VAN SMAALEN, *J. Phys. C: Solid State Phys.* **19,** 5049 (1986).
8. N. LE NAGARD, A. KATTY, G. COLLIN, O. GOROCHOV, AND A. WILLIG, *J. Solid State Chem.* **27,** 267 (1979).
9. H. G. HEIDE, *Ultramicroscopy* **6,** 115 (1981); *Ultramicroscopy* **10,** 125(1982).
10. J. VAN LANDUYT, R. DE RIDDER, R. GEVERS, AND S. AMELINCKX, *Mater. Res. Bull.* **5,** 353 (1970).
11. D. VAN DYCK, C. CONDE-AMIANO, AND S. AMELINCKX, *Phys. Status Solidi A* **56,** 327 (1979); *Phys. Status Solidi A* **58,** 451 (1980).
12. W. L. MCMILLAN, *Phys. Rev. B* **14,** 1496 (1976).
13. C. VAN BRUGGEN, Private communication.
14. E. FLEET, *J. Solid State Chemistry* **62,** 75 (1986).
15. D. VAN DYCK, J. MAHY, R. DEBLIECK, AND S. AMELINCKX, *in* "Proceedings, XI ICEM, Kyoto, 1986," p. 779.